SAND2006-7358C

Compression Creep Behavior of the 95.5Sn-(4.3, 3.9, 3.8)Ag-(0.2, 0.6, 0.7)Cu Solders[1]

Paul Vianco, Jerome Rejent, Alice Kilgo
Sandia National Laboratories
Albuquerque, NM

Joseph Martin
Orion Technologies, Inter.
Albuquerque, NM

ABSTRACT

The compression creep properties were evaluated for the Pb-free solders 95.5Sn-4.3Ag-0.2Cu (wt.%), 95.5Sn-3.9Ag-0.6Cu, and 95.5Sn-3.8Ag-0.7Cu to determine the effects of small composition differences on time-dependent deformation. The test temperatures were -25°C, 25°C, 75°C, 125°C, and 160°C. The nominal applied stresses were in the range of 2 – 45 MPa. Samples were tested in the as-fabricated condition as well as post-aged at 125°C for 24 hours. Negative creep was recorded for all three alloy compositions. However, the extent of this phenomenon was sensitive to alloy composition and the aging treatment. Creep deformation resulted in the formation of coarsened-particle boundaries within the eutectic regions of the microstructure. The boundaries were comprised of Cu_6Sn_5 and, to a lesser extent, Ag_3Sn particles. The minimum creep rate kinetics were evaluated for these solders. The sinh term exponent, n, was 4 – 6 for the Sn-Ag-0.2Cu and Sn-Ag-0.6Cu solders and 1 – 2 for the Sn-Ag-0.7Cu alloy. The apparent activation energy (ΔH) values were in the range of 30 – 70 kJ/mol for all alloys, indicating that a short-circuit or fast-diffusion mechanism controlled creep deformation. The aging treatment did not consistently alter the rate kinetics parameters amongst the alloys. Separating the minimum creep rate data into the low and high temperature regimes, [-25°C, 75°C] and [75°C, 160°C], respectively, showed that bulk diffusion contributed to creep in the higher temperature regime. The ΔH values for the low temperature regime, which indicated that creep was dominated by a fast-diffusion mechanism, were sensitive to solder composition.

INTRODUCTION

The development of Pb-free soldering technology has included a number of studies investigating different alloy compositions as replacements for the traditional 63Sn-37Pb (wt.%, abbreviated Sn-Pb) eutectic solder ($T_{eut.}$ = 183°C) in electronics application. Early investigations examined the feasibility of using existing Pb-free compositions, including the low melting temperature 58Bi-42Sn eutectic solder ($T_{eut.}$ = 139°C) or the 91Sn-9Zn alloy ($T_{eut.}$ = 199°C) that has a melting temperature very similar to that of the eutectic Sn-Pb alloy [1, 2]. Studies were performed that also evaluated the higher melting temperature 96.5Sn-3.5Ag ($T_{eut.}$ = 221°C) and

[1] Sandia is a multiprogram laboratory operated by Sandia Corporation, a Lockheed Martin Company, for the US Dept. of Energy's National Nuclear Security Administration under contract DE-AC04-94AL85000.

95Sn-5Sb ($T_{sol.}$ = 232°C; $T_{liq.}$ = 240°C) solders were already used in some electronics applications, albeit, to very limited extents [3, 4].

As experience with these alloys grew, follow-on studies were undertaken in which several of these basic compositions were altered through alloy additions, in order to improve their processability as well as reliability. Silver additions were made to the 58Bi-42Sn solder, as well as Bi additions made to the Sn-Zn solders, in order to improve mechanical properties [5, 6]. In the case of the high melting temperature Sn-Ag solder, alloy additions of In, Bi, Cu, and other elements were made, either separately or in various combinations, in an effort to lower the solidus temperature [7 – 9]. An important realization that was garnered from all of these studies was that relatively minor alloy addition (<1 wt.%) could significantly affect the physical properties (melting points, solderability, interface reactions, etc.) and mechanical properties (yield strength, fatigue resistance, etc.) of the solder.

The Sn-Ag-Cu ternary alloy family includes a number of compositions that are currently being evaluated for, or are already being used in, the production of Pb-free electronics. The more commonly cited compositions are: 96.5Sn-3.0Ag-0.5Cu (SAC305), 95.5Sn-3.8Ag-0.7Cu (SAC387), 95.5Sn-3.9Ag-0.6Cu (SAC397), and 95.5Sn-4.0Ag-0.5Cu (SAC405). A similar melting temperature of 217°C has been ascribed to these compositions. In addition, the low-Ag alloy 98.5Sn-1.0Ag-0.5Cu (SAC105) is also receiving attention by the electronics industry. A large number of studies have been performed, which evaluated the physical and mechanical properties of the individual solder compositions [10 – 13]. As is often the case, different test methodologies and inconsistent sample fabrication techniques have made it difficult to identify trends (qualitative or statistically significant) between various compositions used in separate studies. There have been several investigations, which are described in Reference 14, that systematically evaluated the effects of varying Ag content (0 – 4.5%) and Cu content (0 – 3.5%) on the yield strength, tensile strength, and the ductility properties of Sn-Ag-Cu compositions. However, those cited works were limited to experiments performed at room temperature conditions and/or did not address time-dependent, that is, creep deformation.

A thorough understanding of the effects of Sn-Ag-Cu composition variations on time-independent and time-dependent mechanical properties is especially critical for the development of computational models that predict the thermal mechanical fatigue (TMF) of Pb-free solder interconnections. The constitutive equations that underlie these models, calculate a deformation rate as a function of the applied stress and temperature (typically at the nodes of a finite element mesh construct of the solder joint). However, the constitutive equation requires as input parameters, the alloy mechanical properties and, in particular, those properties as a function of temperature, in order to accurately compute deformation within the interconnection.

There are two manners by which the Sn-Ag-Cu solder composition can change in the joint. which must then be taken into account during model development. First, there is the obvious difference between starting alloy composition from the list above. Secondly, there is also the concern for changes to the starting composition as a consequence of the assembly process. For example, the dissolution of Cu from circuit board pads and device leads can potentially alter the composition and thus, the mechanical properties, of the solder in the joint.

A study was initiated at Sandia National Laboratories to compile a database of materials properties for the 95.5Sn-3.9Ag-0.6Cu solder (abbreviated Sn-Ag-0.6Cu) in support of the development of a computational model for predicting the thermal mechanical fatigue (TMF) of Pb-free solder interconnections [15]. During the course of that study, it was deemed prudent to examine the sensitivity of the time-independent (stress-strain) and time-dependent (creep)

properties to Sn-Ag-Cu compositions. Therefore, that test program was extended to include two other solder alloys: 95.5Sn-4.3Ag-0.2Cu (Sn-Ag-0.2Cu) and 95.5Sn-3.8Ag-0.7Cu (Sn-Ag-0.7Cu) alloys. The rational for selecting these particular compositions, together with the Sn-Ag-0.6Cu solder, was based upon the following premises: (1) The Sn content was kept the same so that compositional variations were limited to the minor alloy additions, Ag and Cu. (2) Two conditions of Ag and Cu variations were evaluated; a small variation that exists between the Sn-Ag-0.6Cu and Sn-Ag-0.7Cu solders and the more significant difference between the Sn-Ag-0.6Cu and Sn-Ag-0.2Cu compositions.

The microstructures of the three alloys are shown by the optical micrographs in Figure 1. The imaging technique was differential interference contrast. Each microstructure was comprised of varying extents of Sn-rich dendrites. Between the dendrite arms were eutectic regions of Ag_3Sn particles in essentially a 100 wt.% Sn matrix, since there is negligible solubility of Ag in Sn. Electron probe microanalysis (EPMA) indicated that the Cu component was either in solid solution in the Sn rich phase or was present as very small Cu_6Sn_5 particles distributed uniformly in the latter. The large particles in the Sn-Ag-0.2Cu solder (Figure 1a) were pro-eutectic Ag_3Sn as confirmed by EPMA.

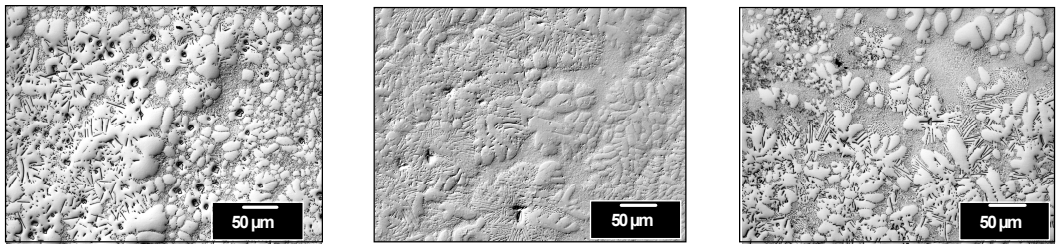

Figure 1 Optical micrographs showing the microstructures of the three solder alloys in the as-fabricated (as-cast) condition: (a) Sn-Ag-0.2Cu, (b) Sn-Ag-0.6Cu, and (c) Sn-Ag-0.7Cu. The micrographs were created by differential contrast imaging.

The results of stress-strain tests were described for the three solder compositions in an earlier report [16]. Briefly, the experimental program used five test temperatures (-25°C, 25°C, 75°C, 125°C, and 160°C); two strain rates (4.2×10^{-5} s^{-1} and 8.3×10^{-4} s^{-1}); and two sample conditions (as-fabricated and aged at 125°C for 24 hours). The purpose of the aging treatment was to determine if it could stabilize the microstructure, which would affect the creep behavior. These temperature conditions were selected to represent likely environments for a solder joint undergoing TMF, either in the field or during accelerated aging tests. The yield strength data is summarized here as this property provided an initial indication of the composition effects.

The yield strength data as a function of alloy composition and test temperature are shown in Figure 2 for the two strain rates. The test samples were in the as-fabricated condition.

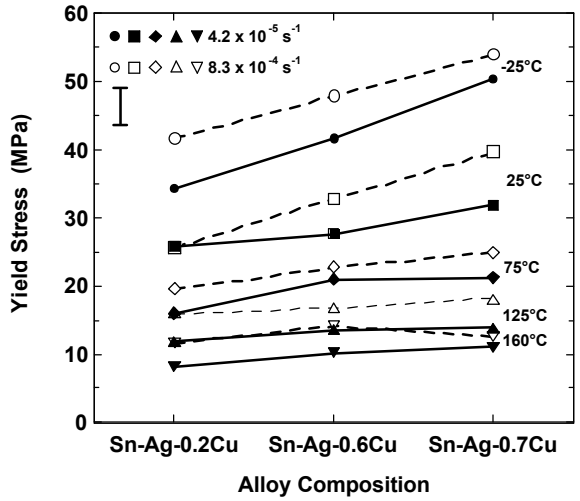

Figure 2 Yield strength as a function of alloy composition and test temperature. The closed symbols refer to the 4.2 x 10^{-5} s^{-1} strain rate. The open symbols are the 8.3 x 10^{-4} s^{-1} strain rate data. The test samples were tested in the as-fabricated condition.

Overall, the trend was for the yield stress to increase with Cu content of the alloy. However, the effect was most significant at the lower test temperatures; it diminished with increasing test temperature. The yield stress increased with strain rate, as expected, for each of the alloys, albeit not to the same degree. However, the sensitivity of yield stress to strain rate became less distinct with increasing test temperature. This trend was observed for all three alloy compositions.

The effects of alloy composition were also examined by comparing data obtained from samples in the as-fabricated condition versus those exposed to the 125°C, 24 hour aging treatment. The yield stress data are shown in Figure 3 for the 4.2 x 10^{-5} s^{-1} strain rate.

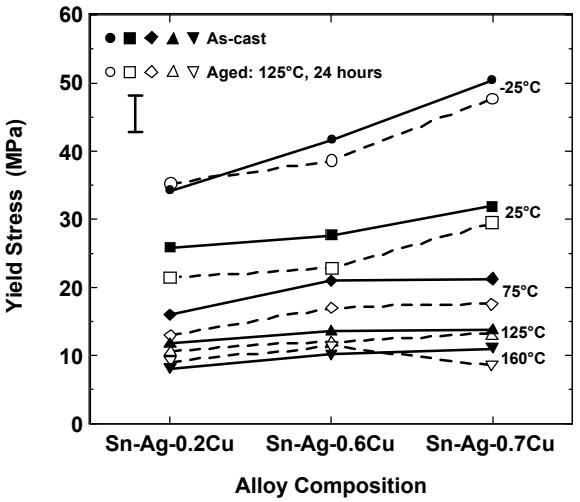

Figure 3 Yield strength as a function of alloy composition and test temperature. The strain rate was 4.2 x 10^{-5} s^{-1}. The test samples were tested in the as-fabricated conditions and after the 125°C, 24 hour aging treatment.

In general, the heat treatment caused a drop in yield stress, which occurred to a greater degree for the Sn-Ag-0.6Cu alloy than for the other two solders. This difference of yield stress values diminished with increased test temperature. The same trends were observed at the faster strain rate, but with a reduced magnitude.

It was clear from yield strength data represented by Figures 2 and 3, as well as the static modulus data that was discussed in Reference 16, that the mechanical properties were sensitive to the relatively small composition differences between the three alloys. Moreover, that sensitivity appeared to be more pronounced at both lower strain rates and reduced test temperatures, conditions that are particularly applicable to engineering applications. The latter observation suggested that the effects of small composition differences could potentially be significant for time-dependent (creep) deformation. Therefore, a study was conducted to compare the creep properties between the same three Pb-free alloys. The analysis assessed the deformation rate kinetics, based upon the minimum or steady-state creep rate, $d\varepsilon/dt_{min}$. The evaluation included an examination of the test sample microstructures. The results of that study are described below.

EXPERIMENTAL PROCEDURES

Test samples

The solder compositions (wt.%) were 95.5Sn-4.3Ag-0.2Cu (abbreviated Sn-Ag-0.2Cu), 95.5Sn-3.9Ag-0.6Cu (Sn-Ag-0.6Cu), and 95.5Sn-3.8Ag-0.7Cu (Sn-Ag-0.7Cu). The sample geometry was a right cylinder having the nominal dimensions of 10 mm diameter and 19 mm length. These dimensions conformed to the "short length" ratio of 2.0 per the ASTM E9-89A test specification [17]. A density determination was made of each specimen to assure that significant voids were not present. A detailed description of the sample fabrication equipment and procedures is available in Reference 15. The specimens were tested in the as-fabricated (as-cast) condition or following an air aging treatment at 125°C for 24 hours.

Creep tests

Creep tests were performed on a servo-hydraulic test frame under constant load control. Duplicate specimens were tested under all stress and temperature combinations. The test temperatures were: -25°C, 25°C, 75°C, 125°C, and 160°C (±0.5°C). The constant load values, which were converted to applied stresses, were selected, based upon 20%, 40%, 60%, and 80% of the nominal yield stress of that alloy at the designated test temperature ($\sigma_{y,T}$). The duration of the creep tests was limited to either a maximum strain of 0.20 or test time of 1.7×10^5 s (approximately two days). Details of the data conditioning, including error analysis, were described in Reference 15.

Data analyses

The strain-time curves were analyzed for qualitative trends as well as quantitatively using the minimum (or steady-state) creep rate, $d\varepsilon/dt_{min}$. The value of $d\varepsilon/dt_{min}$ was determined from each creep test. The "sinh" law equation (1) was used to describe the minimum creep rate as a function of the applied stress, σ (MPa) and test temperature, T (K):

$$d\varepsilon/dt_{min} = A \sinh^n (\alpha\sigma) \exp(-\Delta H/RT) \quad (1)$$

The other variables in equation (1) are as follows: A is a constant (s^{-1}); n is the sinh term exponent; α is the stress coefficient (MPa^{-1}); ΔH is the apparent activation energy (kJ/mol); and R is the universal gas constant (8.314 kJ/mol-K). The sinh law equation was preferred because, as one equation, it can encompass strain rates generated by a wide range of applied stresses without the so-called "power-law breakdown" behavior that is observed with single power-law equations. The parameters A, p, and ΔH were determined from a multivariable, linear regression analysis performed on the logarithm of equation (1). The term $\ln(d\varepsilon/dt_{min})$ was the dependent variable while $\ln[\sinh(\alpha\sigma)]$ and 1/T were the independent variables. The coefficients of the independent variables were n and $\Delta H/R$, respectively. The constant was lnA. The error terms of these parameters were based upon a 63% confidence interval. The regression analysis was performed for different values of the stress coefficient, α. The optimum value of α, which was determined to within $\pm$0.0005, was that which maximized the square of the correlation coefficient (R^2).

RESULTS

Strain-time creep curves

The strain-time curves exhibited largely the primary creep stage leading into steady-state creep for all stresses and temperatures of the as-fabricated, Sn-Ag-0.2Cu solder. The aging treatment resulted in only one instance in which the tertiary stage was a significant part of the deformation. The Sn-Ag-0.6Cu and Sn-Ag-0.7Cu materials exhibited greater contributions of the tertiary stage. Shown in Figure 4 are representative strain-time curves from Sn-Ag-0.7Cu samples tested in the as-fabricated condition.

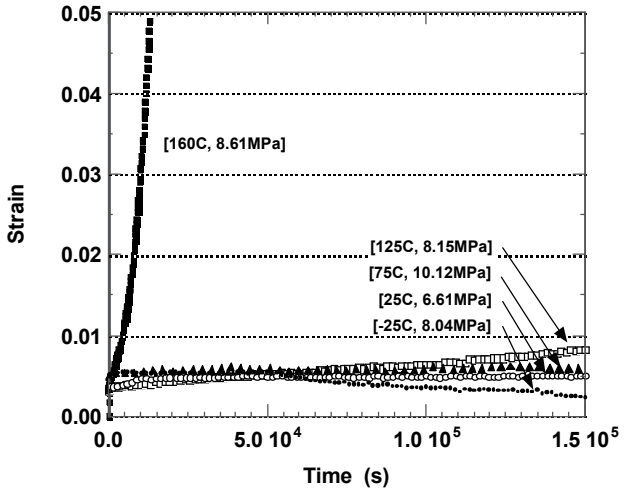

Figure 4 Strain versus time creep curves from Sn-Ag-0.7Cu alloy samples in the as-fabricated condition. The respective stress and temperature parameters are provided in the graph.

When the tertiary stage did occur, it was not accompanied by observable cracking or other discontinuities. Of course, there was an understanding that this level of damage would be less significant in a compression test regiment. The aging treatment did not appear to significantly affect the occurrence of tertiary creep.

The phenomenon of negative creep was observed in several creep curves belonging to the Sn-Ag-0.6Cu solder [15]. Negative creep, as a phenomenon unto itself, has been investigated by other authors [18 – 20]. An example of negative creep appears in Figure 4 for the -25°C, 8.04 MPa test condition (Sn-Ag-0.7Cu; as-fabricated). The frequency of negative creep was assessed by compiling plots of strain rate as a function of applied stress and temperature for all three solder alloys. The tests of both as-fabricated and aged specimens were considered. It was not possible to develop any general trends that crossed all three solder compositions. The Sn-Ag-0.2Cu and Sn-Ag-0.6Cu samples clearly showed an increased occurrence of negative strain rates after aging. The trend was most dramatic for the Sn-Ag-0.6Cu solder as illustrated by the two graphs in Figure 5. In the aged specimens, negative creep occurred primarily at the 75°C test temperature. In the case of the Sn-Ag-0.2Cu samples, the negative strain rates were observed primarily in tests performed at -25°C and 25°C; only one occurrence was recorded at each of the 75°C and 160°C test temperatures. Nearly the opposite trend was observed for the Sn-Ag-0.7Cu solder. A greater frequency of negative creep was observed for the as-fabricated condition than with aged samples. But, the aging treatment only reduced the frequency and magnitude of the negative strain rate for 25°C and higher test temperatures; the aging treatment did not alter the high frequency of negative creep at the -25°C. In general, the aging treatment caused negative creep to occur at lower applied stresses than were observed for the as-fabricated condition.

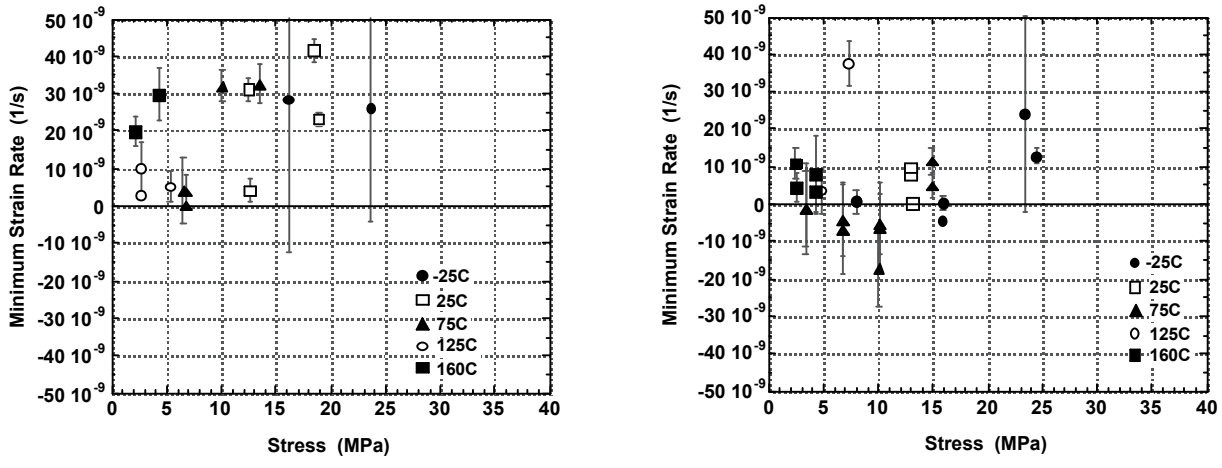

Figure 5 Minimum strain rate as a function of applied stress for the Sn-Ag-0.6Cu alloy samples: (a) as-fabricated condition and (b) after aging at 125°C for 24 hours.

Microstructures

The test sample microstructures were evaluated by metallographic cross sections in order to document the effects, if any, attributed to the creep deformation and, in particular, tertiary creep.

Cracks or voids were not observed in the microstructures of any of the test samples, in spite of strains reaching 0.28 in some tests. The predominant microstructural change was the development of coarsened-particle boundaries within the eutectic regions. This phenomenon is illustrated by the optical micrograph (bright field) in Figure 6.

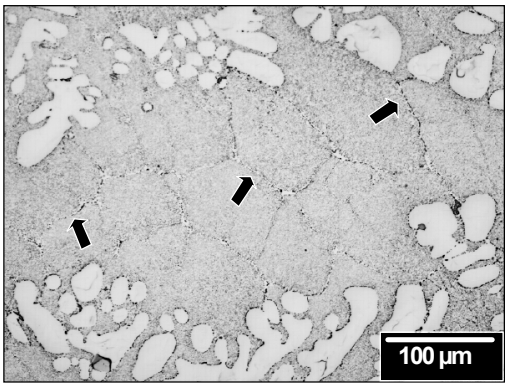

Figure 6 Optical micrograph showing development of coarsened-particle boundaries (arrows) in the eutectic regions of the Sn-Ag-0.7Cu sample (as-fabricated condition). The test temperature, applied stress, strain, and minimum strain rate were: 160°C, 8.61 MPa, 0.1143, and 1.4 x 10^{-6} s^{-1}, respectively.

The Sn-Ag-0.7Cu sample was tested in the as-fabricated condition at 160°C under a stress of 8.61 MPa. The strain (ε) and $d\varepsilon/dt_{min}$ were 0.1143 and 1.4 x 10^{-6} s^{-1}, respectively. The coarsened-particle boundaries were observed at all test temperatures. However, the magnitude of particle coarsening within the boundaries decreased from high to low test temperatures. This point is illustrated in Figure 7.

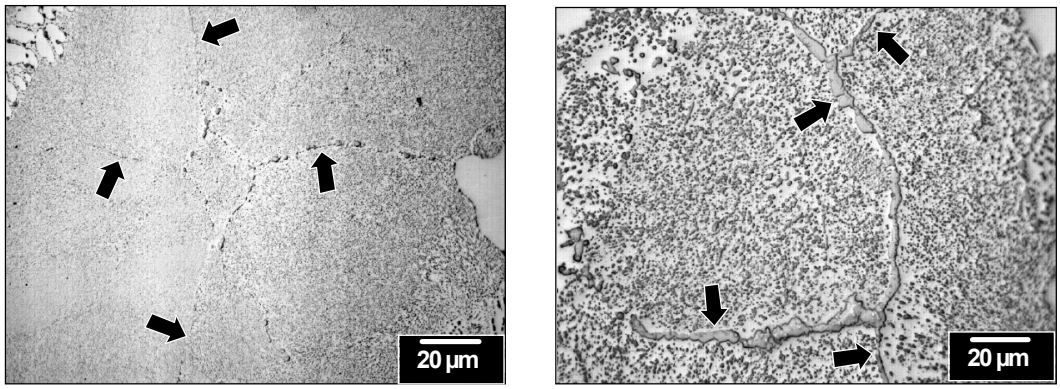

Figure 7 Optical micrographs showing the different magnitudes of particle coarsening in the boundaries (arrows) of two Sn-Ag-0.7Cu samples (as-fabricated condition). The test parameters were as follows: (a) 25°C; 39.5 MPa; ε, 0.122; and $d\varepsilon/dt_{min}$, 2.5 x 10^{-5} s^{-1}. (b) 125°C; 10.9 MPa; ε, 0.119; and $d\varepsilon/dt_{min}$, 2.1 x 10^{-7} s^{-1}.

The micrograph in Figure 7a shows coarsened boundaries (arrows) comprised largely of isolated particles. This morphology was also observed for samples tested at -25°C and 75°C. At the higher test temperatures of 125°C (Figure 7b) and 160°C, the particles within the boundaries coarsened further, forming a contiguous precipitate at many locations. There was not an obvious correlation between the coarsened-particle boundary morphology and either strain or strain rate. Also, there was general coarsening of the Ag_3Sn particle at the elevated test temperatures.

The coarsened-particle boundary phenomenon was observed in the Sn-Ag-0.6Cu samples as reported in Reference 15. A follow-on analysis of those data confirmed that the same morphology dependence on test temperature occurred with that alloy as is illustrated in Figure 7. In addition, the boundaries were largely absent from the as-fabricated Sn-Ag-0.6Cu samples tested at temperatures below 75°C. In the case of the Sn-Ag-0.2Cu samples, the eutectic regions were considerably smaller in size. The development of coarsened-particle boundaries in these regions either did not occur or did so to only a very limited extent. A similar trend was also observed in the other Sn-Ag-Cu samples. The prevalence for the coarsened-particle boundaries appeared to be primarily a function of test temperature; it was less sensitive to applied stress, strain, and strain rate.

It was necessary to determine whether the source of the coarsened-particle boundaries was only the test temperature environment or a consequence of the creep test as a whole, i.e., stress and temperature. Shown in Figure 8 is an optical micrograph of the sample tested at 160°C and a stress of 8.63 MPa.

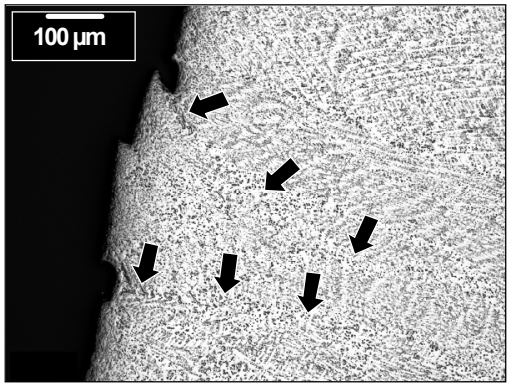

Figure 8 Optical micrograph showing the development of coarsened-particles associated with the bands of shear deformation at the edge of the sample. The test parameters were: (a) 160°C; 8.63 MPa; ε, 0.280; and $d\varepsilon/dt_{min}$, 9.3 x 10^{-7} s^{-1}.

Deformation or shear bands (arrows) developed at the cylinder edge. The shear bands are delineated by narrow regions of coarsening particles. The extent of coarsening was greatest at the sample edge, where deformation was a maximum, and the particles were nearly contiguous (left-most arrow). Towards the interior of the specimen, coarsening diminished as deformation dissipated into the remaining sample volume. The presence of coarsened-particles along the deformation bands correlated this phenomenon to deformation rather than solely being an artifact of the elevated temperatures.

The physical pattern of the coarsened boundaries (e.g., Figure 6) suggested that they coincided with sub-grain or grain development. And, in fact, using the bi-refringence property of Sn, it was confirmed that the coarsened boundaries were located between sub-grains within

those eutectic regions. However, spot EPMA data determined that the coarsened-particles were predominantly the Cu_6Sn_5 composition. There were some Ag_3Sn particles residing with them. One mechanism suggests that sub-grains developed as a consequence of dislocation motion within the Sn matrix of the eutectic regions. The moving dislocations transported Cu atoms (not Cu_6Sn_5 particles) to the sub-grain walls, where they precipitated from solution, creating the coarsened Cu_6Sn_5 particles. In addition, the formation of the sub-grain boundaries by dislocation movement caused a mass transport of Sn that displaced nearby Ag_3Sn particles towards the boundary with the Cu_6Sn_5 precipitates, creating the depleted region to either side of that boundary.

As a final note, the correlation between the coarsened boundaries and the development of sub-grains or grains also established an explanation for the absence of these structures in the Sn-Ag-0.2Cu samples or the smaller eutectic regions of the other compositions. Those eutectic regions were too small to support (thermodynamically) the creation of sub-grain walls by dislocation motion. Therefore, Cu atoms and Ag_3Sn particles were unable to accumulate into the coarsened-particle boundaries.

Steady-state creep rate kinetics

The minimum creep rate kinetics were calculated for each test specimen. The results are presented in the format of equation (1). Again, the error terms on n and ΔH were the 63% confidence intervals. Similar error terms were determined for the constant, A. However, the latter error terms were computed on a logarithm of A so that the 63% confidence interval extended over several orders of magnitude. Because the discussion will center upon the behaviors of n and ΔH, the confidence intervals of A were not recorded in the equations, below.

Sn-Ag-0.2Cu

As-fab. ($R^2 = 0.85$): $d\varepsilon/dt_{min} = 858 \sinh^{4.26\pm0.26}(0.0940\sigma) \exp(-66\pm5/RT)$ (2)

Aged ($R^2 = 0.73$): $d\varepsilon/dt_{min} = 858 \sinh^{4.23\pm0.42}(0.0960\sigma) \exp(-57\pm6/RT)$ (3)

Sn-Ag-0.6Cu

As-fab. ($R^2 = 0.53$): $d\varepsilon/dt_{min} = 4.41\times10^{5} \sinh^{4.18\pm0.63}(0.0050\sigma) \exp(-45\pm7/RT)$ (4)

Aged ($R^2 = 0.69$): $d\varepsilon/dt_{min} = 3.46\times10^{7} \sinh^{5.33\pm0.56}(0.0050\sigma) \exp(-49\pm5/RT)$ (5)

Sn-Ag-0.7Cu

As-fab. ($R^2 = 0.72$): $d\varepsilon/dt_{min} = 0.104 \sinh^{1.96\pm0.21}(0.1735\sigma) \exp(-53\pm7/RT)$ (6)

Aged ($R^2 = 0.41$): $d\varepsilon/dt_{min} = 3.90\times10^{-4} \sinh^{1.34\pm0.27}(0.1560\sigma) \exp(-32\pm7/RT)$ (7)

The goodness-of-fit in the regression analyses, as indicated by the R^2 value, varied considerably between the different alloys. Moreover, the aging treatment did not have a consistent effect on R^2. In the case of the Sn-Ag-0.2 and Sn-Ag-0.7Cu alloys, the aging treatment resulted in worse regression correlations; the opposite effect was observed for the Sn-Ag-0.6Cu solder. These observations imply that, in fact, this aging treatment did not stabilize the microstructure with the intent of providing more consistent mechanical properties.

The values of n and ΔH were evaluated. The interpretation of the sinh term exponent, n, must account for the fact that it incorporates both low stress (n = 1 – 3) and high stress (n = 7 – 10) regimes. Values of n equal to 4 – 6 imply that both regimes are generally contributing to the

creep behavior. Therefore, the values of 1.96 and 1.34 suggested that a viscous flow mechanism, which has a more limited sensitivity to stress, governed the creep of Sn-Ag-0.7Cu solder. However, the values of ΔH indicated that the viscous flow mechanism was based upon short-circuit or fast-diffusion paths for the transport of atoms required to support the deformation. Typically, fast diffusion goes hand-in-hand with grain boundary diffusion. Certainly, it can be argued that the short-circuit diffusion mechanism coincided with the formation of the sub-grain structure as indicated by the coarsened-particle boundaries; those boundaries and related sub-structures – e.g., particle/Sn interfaces and nearby depletion zone) provided the pathways.

The values of n and ΔH as a function of alloy composition are shown in Figure 9. The plot in Figure 9a represents the as-fabricated condition; the plot in Figure 9b is for the aged condition. It was interesting to note that the heat treatment had a significant effect on only the Sn-Ag-0.7Cu parameters per the 63% confidence interval, particularly, the decrease in the ΔH values after aging. A smaller decrease was observed for the value of n. In the absence of a more detailed microstructural analysis, the drops in n and ΔH values would suggest that the sub-grain and grain boundary development may have actually begun to develop, although to a limited extent, during the aging treatment, prior to administering the applied stress.

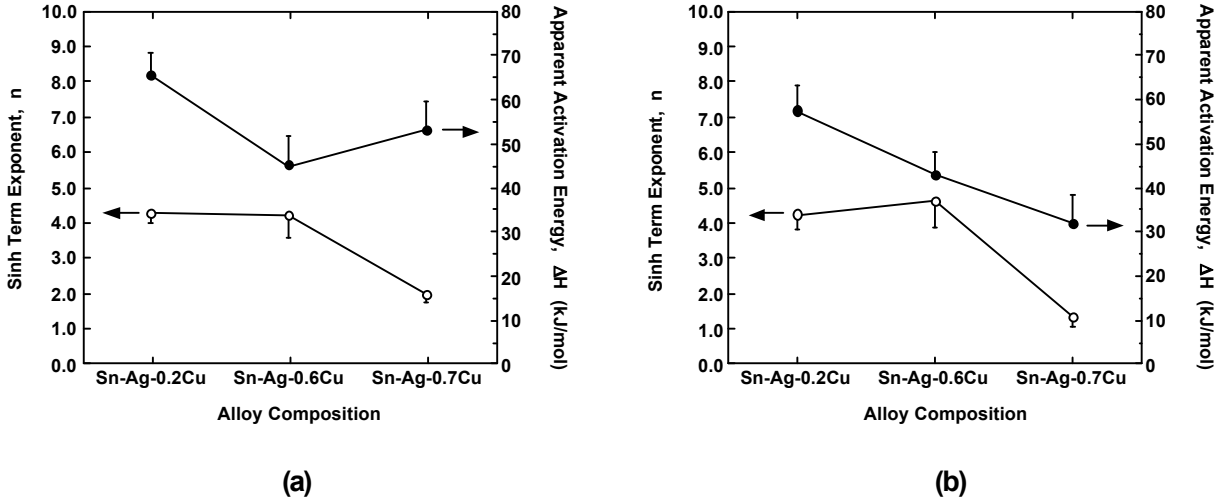

Figure 9 Graphs of the kinetics parameters, n and ΔH, as a function of alloy composition: (a) as-fabricated condition and (b) specimens aged at 125°C for 24 hours.

Further analyses were performed on the minimum strain rate data. Because the R^2 values are relatively low in several cases, it is necessary to determine if the poor correlation was due to a temperature dependence of the rate kinetics. This dependency most often appears in the apparent activation energy, ΔH, which signifies a change of controlling mechanism. The strain rate data were split into a low temperature regime [-25°C, 75°C] and high temperature regime [75°C, 160°] as was similarly done in the Reference 15. The regimes overlapped at 75°C. The minimum creep rate kinetics were recalculated separately for both regimes using two approaches. The first approach kept the value of α unchanged from that calculated initially using data representing the combined temperature regime, [-25°C, 160°C]. The second approach was to recalculate α separately for each of the two temperature regimes, using the value that maximized R^2. The corresponding kinetic parameters were documented. The discussion will be limited to the as-fabricated condition; similar behaviors were observed for the aged samples.

Separating the minimum creep rate data into the two temperature regimes resulted in higher R^2 values for each of the two separate cases. The differences were greatest for the Sn-Ag-0.6Cu solder and least significant for the Sn-Ag-0.2Cu alloy. Shown in Figure 10 is a graph of the apparent activation energy (ΔH) as a function of solder alloy composition and temperature regime for the as-fabricated samples. Recomputing α had minimal impact on the ΔH values. It appears that the creep deformation was a combination of a high temperature and a low temperature mechanism. The values of ΔH for the high temperature regime suggested bulk diffusion as the controlling mechanism. Typical values for this mechanism are 90 – 110 kJ/mol [21]. Referring to coarsened-particle boundary formation in Figures 6 and 7, diffusion-based dislocation motion (climb) at the elevated temperatures would be a likely process to support this phenomenon and associated sub-grain development. The mechanism controlling creep at low temperatures and, which also dominated the overall (combined temperature regime) kinetics, was short-circuit or fast diffusion. Moreover, it was the low temperature creep behavior that distinguished the three alloy compositions and, by inference, the associated microstructures. Therefore, composition differences between Sn-Ag-Cu alloys appears to affect creep more so at the low temperatures, that is, below approximately 75°C. At higher temperatures, compositional or microstructural differences have a lesser role as bulk diffusion becomes the controlling mechanism. Lastly, the sensitivity of creep properties to solder composition occurs in a temperature and stress space that is important for engineering applications.

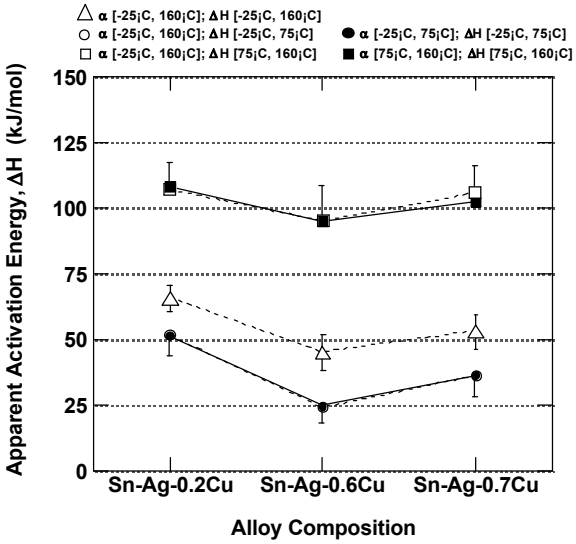

Figure 10 Values of ΔH as a function of solder composition and temperature regime. The values of ΔH that were calculated from the α determined for the combined temperature regime (open symbols) and α values optimized for each separate temperature regime (closed symbols).

CONCLUSIONS

1. Compression creep properties were evaluated for the Pb-free solders 95.5Sn-4.3Ag-0.2Cu (wt.%), 95.5Sn-3.9Ag-0.6Cu, and 95.5Sn-3.8Ag-0.7Cu to determine the effects of small alloy composition differences. The test temperatures were -25°C, 25°C, 75°C, 125°C, and 160°C. The nominal applied stresses were 2 – 45 MPa. Samples were tested in the as-fabricated condition as well as after aging at 125°C for 24 hours.

2. Previous studies determined that the time-independent (stress-strain) mechanical properties were sensitive to the composition differences between these three solders. That sensitivity was more significant at the lower strain rate and reduced temperatures.
3. Negative creep was recorded for all three alloy compositions. However, the extent of this phenomenon depended upon use of the aging treatment and alloy composition.
4. Creep deformation resulted in the formation of coarsened-particle boundaries within the eutectic regions of the microstructure. The boundaries, which were comprised of Cu_6Sn_5 and, to a lesser extent, Ag_3Sn particles, delineated formation of sub-grains or grains.
5. The minimum creep rate kinetics were evaluated by the sinh law. The sinh term exponent, n, was 4 – 6 for the Sn-Ag-0.2Cu and Sn-Ag-0.6Cu solders and 1 – 2 for the Sn-Ag-0.7Cu alloy. The apparent activation energy (ΔH) values were in the range of 30 – 70 kJ/mol for all alloys, indicating that short-circuit or fast-diffusion controlled creep deformation. The aging treatment did not consistently alter the rate kinetics parameters amongst the alloys.
6. Separating the minimum creep rate data into the two temperature regimes [-25°C, 75°C] and [75°C, 160°C], the values of ΔH indicated that bulk diffusion controlled creep in the higher temperature regime. Here, the ΔH values were relatively insensitive to solder composition. However, in the low temperature regime, creep was dominated by the fast-diffusion mechanism and ΔH exhibited a sensitivity to solder composition.

ACKNOWLEDGEMENTS

The authors wish to thank D. Susan for his careful review of the manuscript. Sandia is a multiprogram laboratory operated by Sandia Corporation, a Lockheed Martin Company, for the US Dept. of Energy's National Nuclear Security Administration under contract DE-AC04-94AL85000

REFERENCES

1. L. Felton, C. Raeder, and D. Knorr, *J. of Metals,* **45** 28 (1993).
2. C. Chuang, T. Lui, and L. Chen, *J. Elect. Mater.* **30** 1232 (2001)
3. R. Darveaux, *IEEE Trans. CHMT* **15** 1013 (1992).
4. P. Vianco, D. Frear and F. Hosking, in *Materials Developments in Microelectronic Packaging: Performance and Reliability, Proceedings of the Fourth Electronic Materials and Processing Congress*, edited by P. Singh (ASM, International, Materials Park, OH; 1991), pp 373-380.
5. M. McCormick, J. Chen, G. Kammlott, and S. Jin, *J. Elect. Mater.* **26** 954 (1997).
6. P. Harris, *Surf. Mount Tech.,* **11** 46 (1999).
7. N. Lee, J. Slattery, J. Sovinsky, and P. Vianco, *Proc. Surface Mount International* (San Jose, CA, August 28 to September 1, 1994), p. 463.
8. P. Vianco and J. Rejent, *J. of Elect. Mater.* **28** 1131 (1999); ibid, *J. Elect. Mater.* **28** 1139 (1999).
9. P. Vianco, J. Rejent, and R. Grant, *Mater. Trans. of Jap. Inst. of Met., 45* 765 (2004).
10. S. Kung, et al., *Mater. Trans. of Jap. Inst. of Met.,* **45** 695 (2004).
11. M. Rist, W. Plumbridge, and S. Cooper, *J. Elect. Mater.* **35** 1050 (2006).
12. J. Pang and B. Xiong, *IEEE Trans. on CPT* **28** 830 (2005).
13. K.-I. Ohguchi, K. Sasaki, and M. Ishibashi, *J. Elect. Mater.* **35** 132 (2006).
14. *Environmentally Friendly Electronics: Lead-Free Technology,* edited by J. Hwang (Electrochemical Pub., Ltd., Port Erin, UK; 2001) pp. 231 – 243.

15. P. Vianco, J. Rejent, and A. Kilgo, *J. Elect. Mater.* **32** 142 (2003); ibid, *J. Elect. Materials* **33** 1389 (2004); ibid, J. Elect. Materials **33** 1473 (2004).
16. P. Vianco and J. Rejent, *J. of Metals* **55** 50 (2003).
17. *Standard Test Methods for Compression Testing of Metallic Materials at Room Temperature,* **ASTM E9-89A** (American Society for Testing and materials, West Conshohoken, PA, 1995), p. 101.
18. P. Vianco and J. Li, *Mater. Sci. and Eng.* **95** 693 (1987).
19. J. Li, *Mater. Sci. and Eng.* **98** 465 (1988).
20. J. Kirkaldy, *Mater. Sci. and Eng.* **409** 167 (2005).
21. J. Astin, *Tracer Diffusion in Solids* (Plenum, New York, 1970)